A Beehive Inspired Hydrogen Photocatalytic Device Integrating a Carbo- benzene Triptych Material for Efficient Solar Photo-reduction of Seawater

Jérémy Cure, Kévin Cocq, Andréa Nicollet, Kui Tan, Teresa Hungría, Sandrine Assié-Souleille, Séverine Vivies, Ludovic Salvagnac, Manuel Quevedo-lopez, Valérie Maraval, et al.

A Beehive Inspired Hydrogen Photocatalytic Device Integrating a *Carbo*-benzene Triptych Material for Efficient Solar Photo-reduction of Seawater

Jérémy Cure[1,*], *Kévin Cocq*[2], *Andréa Nicollet*[1], *Kui Tan*[3], *Teresa Hungria*[4], *Sandrine Assie-Souleille*[1], *Séverine Vivies*[1], *Ludovic Salvagnac*[1], *Manuel Quevedo-Lopez*[3], *Valérie Maraval*[2], *Remi Chauvin*[2], *Alain Estève*[1], *Carole Rossi*[1,*]

[1] LAAS-CNRS, University of Toulouse, 7 avenue du colonel Roche, 31031 Toulouse, France

[2] LCC-CNRS, University of Toulouse, 205 route de Narbonne, 31077 Toulouse, France

[3] Department of Materials Science and Engineering, University of Texas at Dallas, Richardson, TX (USA)

[4] Centre de Microcaractérisation Raimond CASTAING, University of Toulouse, CNRS, UT3-Paul Sabatier, INP, INSA, Espace Clément Ader, 3 rue Caroline Aigle, 31400 Toulouse, France

Keywords: photocatalytic device, hydrogen production, water splitting, triptych system, *carbo*-benzene dye, gold nanoparticle, titanium dioxide film

Abstract:

The dream to produce green, clean and sustainable hydrogen from earth-abundant and free resources such as seawater and sunlight is highly motivating because of the interest for desirable economical and societal applications in energy. However, it remains challenging to develop an efficient and unassisted photocatalytic device to split seawater molecules with just sunlight without any external bias. For the first time, we develop a such novel hierarchical material based on thin film technology that integrates TiO_2 semiconductor layers, embedded gold nanoparticles and a photosensitive *carbo*-benzene layer. The design of the triptych device placing the photocatalyst in be-to-be increases the photoactive surface area by a factor 2. Its robustness (>120 h), stability (>5 days) and efficiency (STH 0.06%) are measured in NaCl-salted water. The chloride ions act as hole scavengers and induce an increase of pH increasing in turn the sun-driven hydrogen production rate.

Text:

The key for the industrial development of hydrogen production is the development of technology that allows *large-scale and low-cost* production. Traditionally, steam reforming from *fossil fuels* is used for large scale H_2 production.[1-4] However, this produces low purity H_2 with CO and CO_2 contaminants that leads to massive emission of greenhouse gases which are incompatible with the requirement of a sustainable energy source.[5,6] Other routes explored for sustainable hydrogen production include from either biomass[2,3] and water which are abundant on earth.[7-9]

Electrolysis is a well-known method to produce hydrogen when water is used as the source of hydrogen from water splitting. This method allows to produce high quality and pure H_2 that can

be used for sustainable production of electricity. However, electrolysis is energy demanding making the water splitting process economically unattractive for large scale production. An alternative to electrolysis is the unbiased water splitting using sunlight. In this case, sunlight irradiates a photocatalyst dispersed in an aqueous solution and hydrogen can be readily produced.[10-14] Photocatalytic water splitting (PC-WS) is a simple, sustainable and totally carbon-free method that can be envisaged to produce hydrogen at large-scale and low-cost.[15-18] A PC-WS device requires a semiconductor possibly combined to co-catalysts with no need for counter electrode, supporting electrolyte nor pH-buffer to convert photon energy into chemical energy.[19] Schröder *et al* and Goto *et al.* developed the first PC-WS hydrogen panels integrating a particulate form[20] of the photocatalyst, but with scarce elements such as Sr.[19,21,22]

An inherent problem in the design of efficient PC-WS *devices is the mismatch between the solar spectrum and the thermodynamic and kinetic requirements for water splitting reaction*. Most of the semiconductors used for PC-WS (TiO_2, ZnO, etc.) have large band gaps that reduces the amount of light absorbed. Other issues include charge carrier separation and transport.[15,16] In addition, frequently a poor semiconductor stability results in a loss of efficiency after a short period of time.[22-25]

Herein, we describe a novel, safe, green and scalable TiO_2-based PC-WS thin film system featuring Au nanoparticles embedded into the semiconductor and covered with a photosensitive *carbo*-benzene (Cbz) layer (Figure 1).[26] The novelty and interest of this PC material lie in: (1) the use of Au co-catalyst nanoparticles (NPs) deeply embedded into a crystalline TiO_2 semiconductor film; (2) optimization of Au NPs size and spatial distribution; (3) the final coverage with a layer of Cbz selected for the extremely high single molecule conductance of its *carbo*-aromatic core

(~100 nS)[27] and its high molar extinction coefficient (ε = 131 000 L.mol^{-1}.cm^{-1} at λ_{max} = 493 nm).[28,29] This layer acts both as a photosensitizer and a protective layer against photo-corrosion.[26]

An efficient triptych PC device (T-PC) integrating these three components catalyst onto silicon and glass substrates is described (Figure 4a-c) and used for photo-reduction of water from various aqueous solutions. The device shows a Solar-to-Hydrogen (STH) yield of 0.06% in salted water condition compared to other PC thin films.[20,26,30-39] Altogether, these results open a scalable and inexpensive way for hydrogen production.

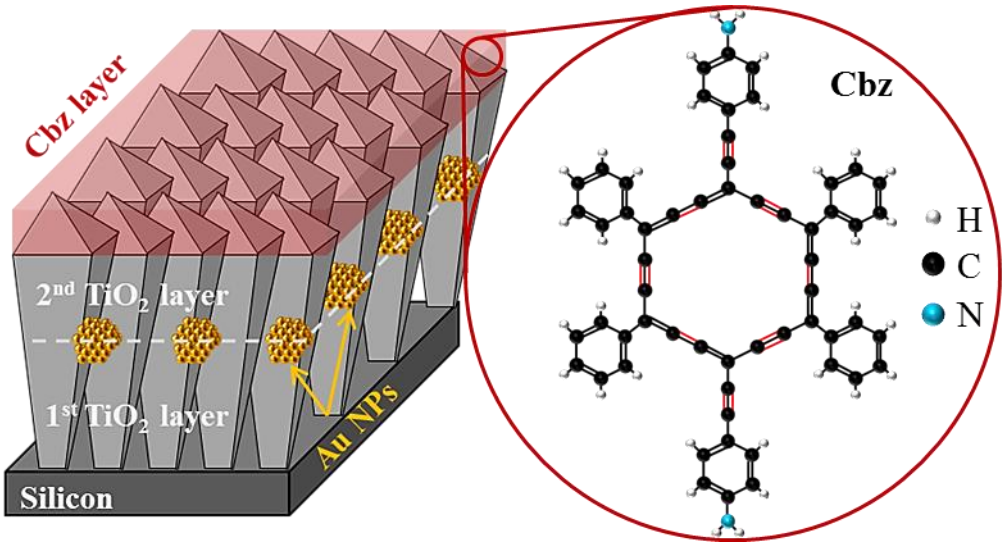

Figure 1. *Scheme of the triptych bilayer material composed (from the bottom to the top) by a first layer of TiO_2 (in light grey), gold nanoparticles (in yellow), a second layer of TiO_2 (in light grey) and a photosensitive layer of Cbz (in red). The inset shows the molecular structure of Cbz.*

Triptych films.

The photocatalytic triptych bilayer film, thereafter named TiO_2/Au/TiO_2/Cbz, consists of a first layer of TiO_2 (270 nm thick), buried Au NPs, a second TiO_2 layer (270 nm thick) and a photosensitive layer of Cbz. All layers are deposited on a silicon substrate (Figure 1). The TiO_2 layers are deposited using magnetron and show a columnar microstructure, comparable to that of TiO_2 anatase films obtained by MOCVD process reported by Miquelot *et al.*[40] Both TiO_2 layers are 84 ± 1% and 16 ± 1% anatase and rutile TiO_2 phases, respectively (see grazing incidence X-ray diffraction (GI-XRD) diagram in Figure 2a). Although Au NP are buried the XRD analyses show gold peaks corresponding to the Au NPs overlapping with the anatase TiO_2 peaks (Figure 2a). Nonetheless, the first ~20 nm of TiO_2 deposited on the substrate silicon surface are amorphous (see supporting information SI, Figure S3). A columnar polycrystalline TiO_2 film grow on top of this first layer during the deposition and generate porosities (~1-10 nm) which are observed between the columns by high-angle annular dark-field scanning transmission electronic microscopy (HAADF-STEM) (Figure 2d, see SI, Figure S4).

The photo-decomposition of the gold precursor on the surface of the first layer of TiO_2 (270 nm thick) leads to the growth of Au NPs not only on its top surface, but also inside its porosities (see SI, Figure S5a,b). Scanning electronic microscopy (SEM) results show a 20 to 60 nm Au NPs size distribution (inset Figure 2c) with NP areal density of 60 ± 1 NPs/ µm² (Figure 2c). We note that a few Au NPs confined inside the pores of the TiO_2 have a size around ~ 7 nm (see SI, Figure S5b).

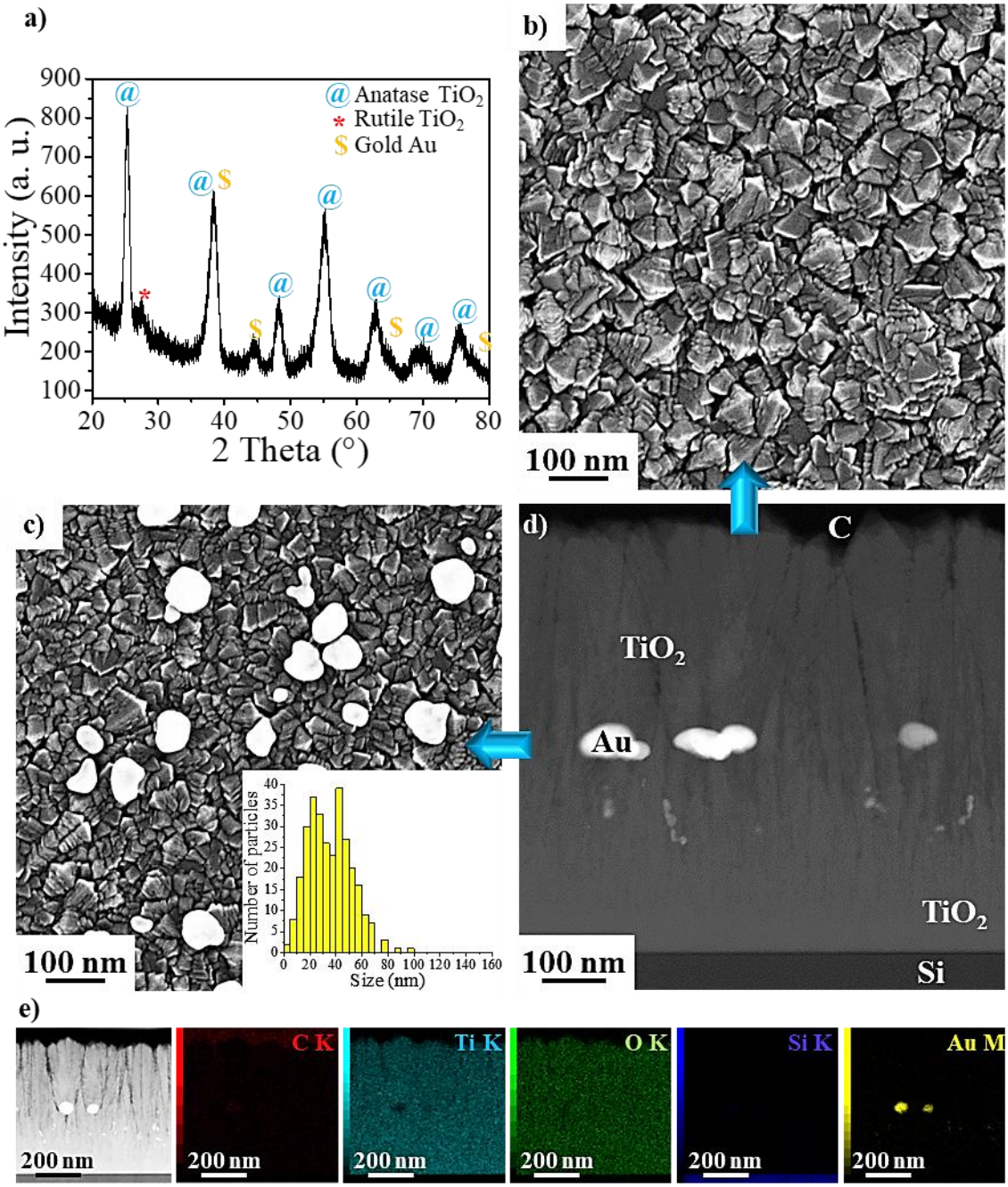

Figure 2. *a) GI-XRD pattern: anatase TiO_2 (blue @), rutile TiO_2 (red *) and Au (orange $) b-d) Microstructure of TiO_2/Au/TiO_2/Cbz material: SEM observation of the top surface of b) the second TiO_2 layer and c) the first TiO_2 layer covered by Au NPs (inset of the size distribution of Au NPs); d) HAADF-STEM cross-section image and e) STEM-EDS mapping of a cross-section of*

TiO_2/Au/TiO_2/Cbz coated with a thin sputtered carbon layer. The following elements are depicted: C (red), Ti (cyan), O (green), Si (blue) and Au (yellow).

The second columnar TiO_2 film grows without any evident interface between the two layers, as observed by HAADF-STEM (Figure 2d). The Au NPs result in broader porosities (Figure 2d, see SI, Figure S5a). No gold diffusion is observed during the deposition of the second TiO_2 layer.

The ~1-2 nm thick photosensitive Cbz layer cannot be identified from SEM. Nonetheless, the increase of the contact angles (measured from a drop of water) after the deposition of the hydrophobic Cbz layer onto the TiO_2 surface from 48.9 ± 1.3° to 86.0 ± 2.3° indicates the presence of such layer, in agreement with the X-ray photoelectron spectroscopy (XPS) results.

The XPS analysis (Figure 3a,b) shows the binding energies for the Ti $2p_{1/2}$, Ti $2p_{3/2}$ and O 1s core levels at 465.2 ± 0.1 eV, 457.0 ± 0.1 eV and 530.0 ± 0.1 eV, respectively. The gold is not detected since it buried inside the TiO_2 layer (Figure 2d,e). The N 1s core level binding energy corresponding to the functional group ($-NH_2$) of the photoactive Cbz molecule (Figure 3d) is evidenced at 400.7 ± 0.1 eV, typical for Cbz molecules in interaction with a metal oxide surface.[26] Note that the weak intensity of the N 1s signal is due to the very thin layer of Cbz onto the TiO_2 surface. These results confirm the composition of the semiconductor TiO_2 layer and the deposition of the Cbz photosensitive layer onto the surface of the TiO_2/Au/TiO_2/Cbz material according to our previous studies.

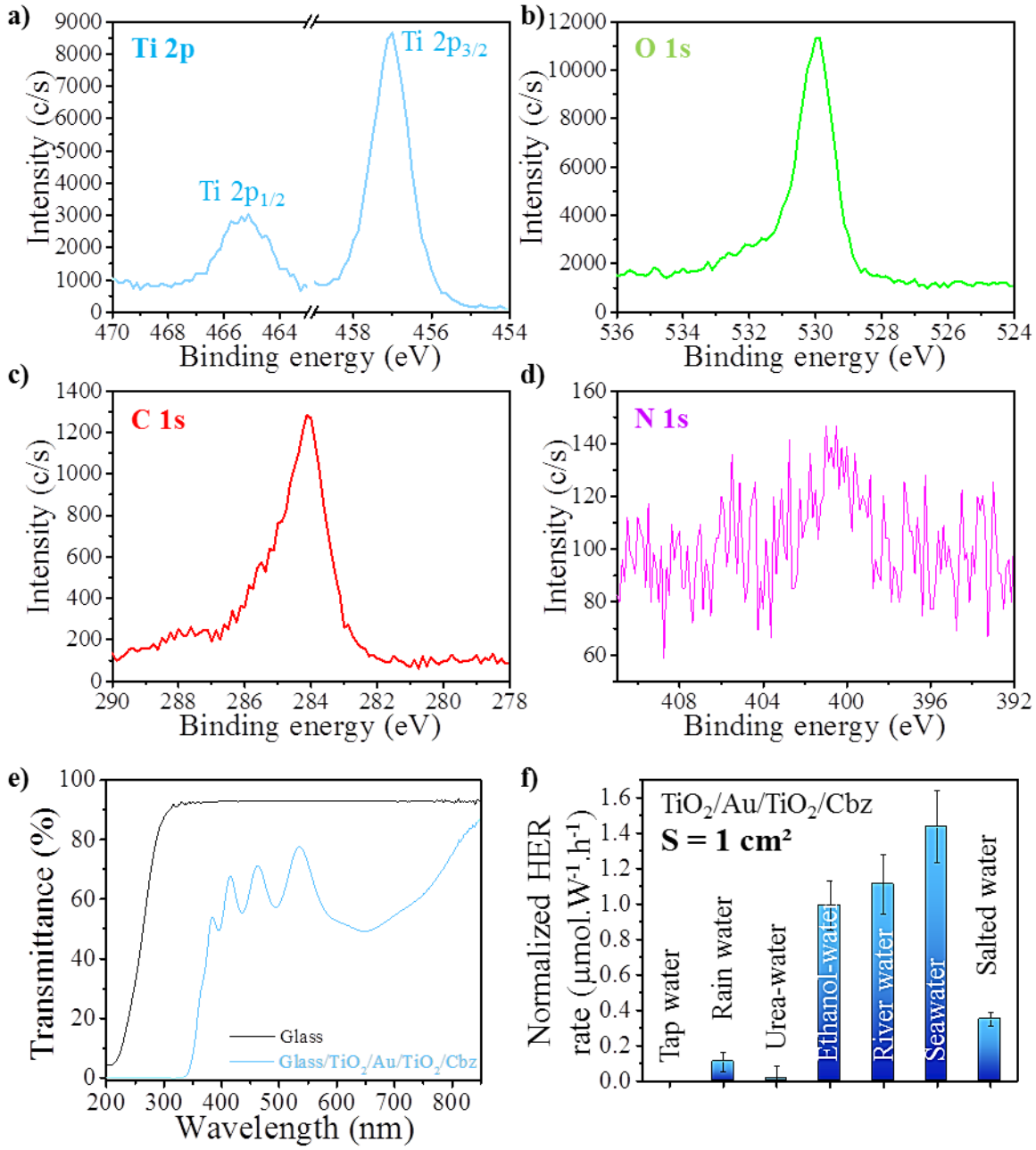

Figure 3. *XPS spectra of the triptych bilayer TiO_2/Au/TiO_2/Cbz material for the: a) Ti $2p_{3/2,1/2}$ (cyan curve); b) O 1s (green curve); c) C 1s (red curve) and d) N 1s (violet curve) regions; e) transmittance spectra in the 200-850 nm region for the borosilicate glass B33 (black curve) and the triptych bilayer TiO_2/Au/TiO_2/Cbz material deposited onto the glass (cyan curve); f)*

hydrogen production rate (µmol.W^{-1}.h^{-1}) normalized by the light flux and the surface area (cm²). See more experimental details in SI, Section A-4.

The transmittance *T* (%) of the triptych bilayer TiO_2/Au/TiO_2/Cbz is shown with the cyan curve, Figure 3e. For comparison, the transmittance of the glass substrate is also depicted (black curve in Figure 3e). These results evidence the ability of the triptych bilayer material to efficiently absorb visible light, which is expected to increase the photocatalytic performance. The decrease of transmittance between 400 and 200 nm results from the fundamental absorption of light according to the TiO_2 bandgap. The bands in the 550-400 nm region correspond to constructive and destructive interferences related to the film thickness and the difference in refractive index between the TiO_2 film and the glass substrate.[41] Finally, the decrease of transmittance in the 850-550 nm region may result from the deposition of the second TiO_2 layer (see SI, Figure S6).

The photocatalytic performance of the TiO_2/Au/TiO_2/Cbz material deposited on silicon (substrate surface areas: S =1 cm²) was then investigated in various aqueous media (Figure 3f): ethanolic solution (35% ethanol + 65% deionized (DI) water, in volume), tap water, rain water, seawater, salted water (pure NaCl diluted in DI water with a concentration close to that of ocean *i.e.* [NaCl] = 35 g/L), river water, and urea solution (pure urea diluted in DI water with a concentration close to that of the human urine *i.e.* [urea] = 400 mmol/L). The hydrogen evolution reaction (HER) rates are normalized with respect to the light flux received by the sample (see SI, Section B-3.1, Figure 3f) and calculated after 24 h of stabilization of the system under illumination (Xenon lamp, 300 W, wavelength range: 300-1100 nm), the H_2 production being linear (see SI, Section B-3.2).

Tap and rain water as well as urea do not yield a high hydrogen evolution reaction (HER) rate, as compared to the other aqueous media with values of: 0, 0.11 ± 0.05 and 0.02 ± 0.06 µmol.W^{-1}.h^{-1}, respectively. The weak performance of the photocatalyst in tap and rain water and urea is probably due to the absence of pollutants able to play the role of holes scavengers. Indeed, the addition of hole scavengers in water was reported to enhance the H_2 production from water.[42,43] Note that urea is not an efficient hole scavenger for the TiO_2/Au/TiO_2/Cbz photocatalyst, while it was described to be for other PC materials.[44] Ethanol can be considered as an organic pollutant model and its addition (35% in volume) in water is indeed found to increase the HER rate from 0 to 0.99 ± 0.14 µmol.W^{-1}.h^{-1} (Figure 3f). For the sea and river water media, the normalized HER rates are quite similar: 1.43 ± 0.20 and 1.11 ± 0.17 µmol.W^{-1}.h^{-1}, respectively, but the H_2 production is accompanied with CO_2 production which may result from the photo-degradation of pollutants (see SI, Section B-3.3) and happens to not be compatible with the requirement of a green H_2 production. Finally the use of salted water is an alternative to the addition of ethanol giving a HER rate of 0.35 ± 0.04 µmol.W^{-1}.h^{-1} (Figure 3f).

To the best of our knowledge, only very few unassisted PC-WS systems, i.e. photocatalysts without any external bias, are reported in the literature. In addition, inspection of the state of the art shows that the use of thin film technology in pure photocatalysis is a very recent idea, initially reported by Gopinath *et al.* in 2019.[20] A table summarizing the most relevant published works on thin film catalysts is given in the SI, Section B-4).[20,26,30-39] Although systematic comparison is difficult due to the variability of the parameters and missing information (working pressure and temperature, aqueous medium, hole scavenger, irradiation conditions, etc.), the performance of our triptych system is equivalent to that of previously reported PC thin films, but under the most

drastic conditions ever investigated in the literature (low light flux: 12 $mW.cm^{-2}$ and high pressure: 2.0 bar), i.e. closer to the applications (see SI, Section B-4).

T-PC device for solar PC production of H_2

This section focuses on the performance of the PC device in ethanol-water and salted water media. For this study, the T-PC device is manufactured in aluminum and covered by a glass of borosilicate B33 (4 mm thick, 120 mm diameter, Figure 4a-c) to ensure light penetration and airtightness, two important parameters since H_2 is produced inside the device. A first plate of TiO_2/Au/TiO_2/Cbz material deposited on a silicon substrate (5 x 5 cm) is placed at the center of the T-PC device (Figure 4a-c). A second plate of similar TiO_2/Au/TiO_2/Cbz constitution deposited on a glass wafer of borosilicate B33 (100 mm diameter) is placed in parallel of the first plate: the thickness of the first layer of TiO_2 is 1070 nm (Figure 4c), the optimal thickness in terms of H_2 production for a single layer of TiO_2 deposited on glass B33 (instead of 270 nm in the first plate: Figure 4c). This unprecedented setup allows increasing the photoactive surface by a factor 2 in the final T-PC device, compared to others photocatalytic thin films developed to date.[19,21] Finally, the T-PC device (V = 23.2 cm^3) is filled with aqueous solutions leading to a coverage of the photocatalytic material by 4 mm of water (Figure 4a-c), which was estimated to be a compromise between the amount of water required for photocatalysis and an appropriate weight for final application on houses roofs.[19]

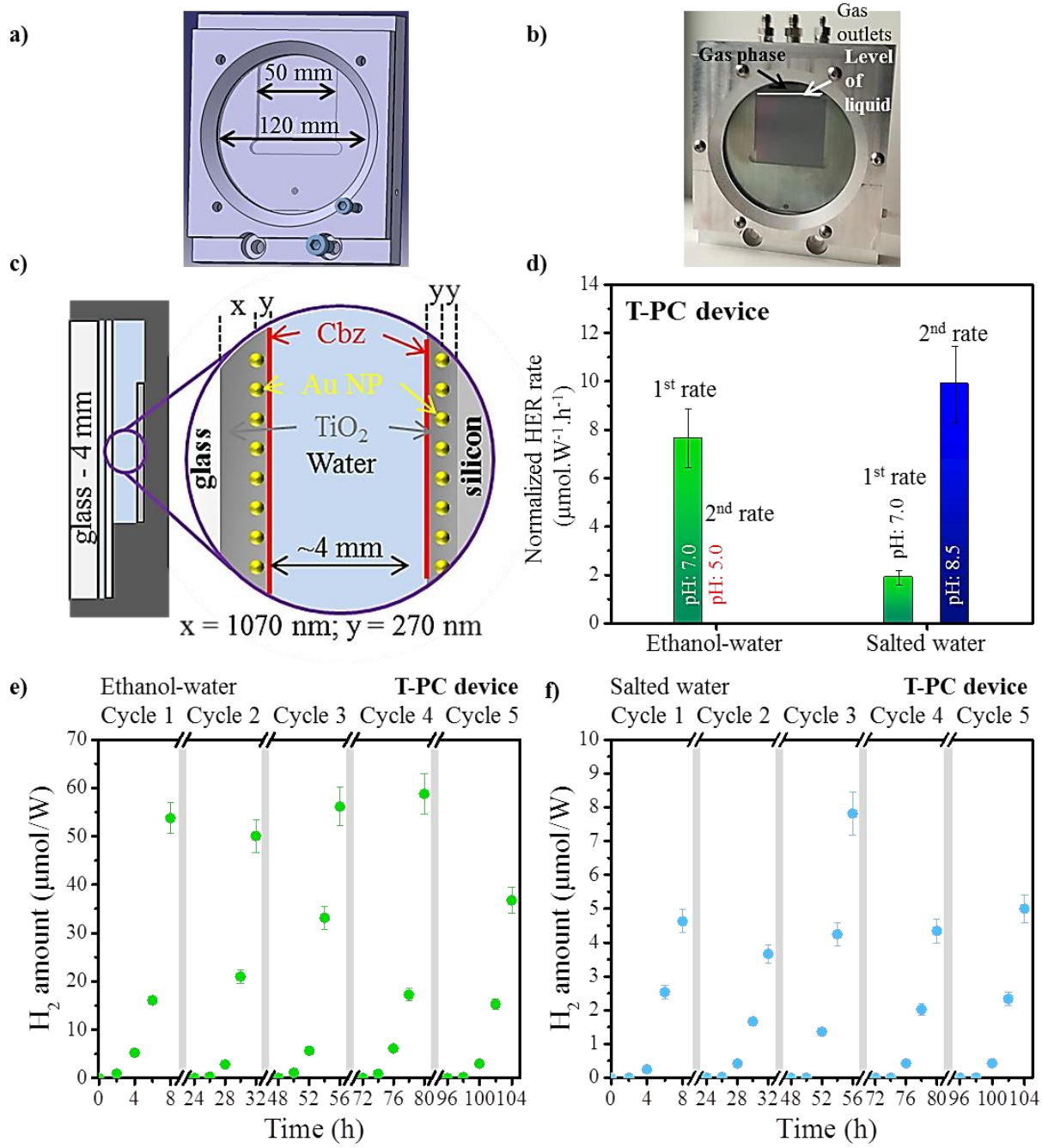

Figure 4. *a) Front schematic view, b) optical image and c) profile schematic view of the T-PC device (from the left to the right: a 4 mm-thick glass (light grey), the TiO_2/Au/TiO_2/Cbz material deposited on glass (light grey) and on silicon (dark grey) respectively, which are immersed in water (light blue)). The Au NPs and Cbz layer are depicted in yellow and red, respectively. The x*

and y values are the thicknesses of the two TiO_2 layers. d) Normalized hydrogen production rates from ethanol-water and salted water media for two successive photocatalytic regimes (1^{st} and 2^{nd} rates) correlated with a change in pH: initially neutral (green bars), then acidic (red bars) or basic (blue bars). Cyclability of H_2 production in the T-PC device under visible light irradiation for: e) a 35:65 ethanol:deionized water solution (green circles) and f) a salted water solution ([NaCl] = 35 g/L, blue circles). See more experimental details in SI, Section A-4.

The use of the T-PC device based on this thin films technology (Figure 4a-c) leads to an enhancement of the H_2 production by a factor 7.7 (7.6 µmol.W^{-1}.h^{-1}) in ethanol-water, and 5.4 (1.9 µmol.W^{-1}.h^{-1}) in salted water (Figure 3f) compared to the single TiO_2/Au/TiO_2/Cbz material on Si wafer: (0.99 ± 0.14 µmol.W^{-1}.h^{-1} and 0.35 ± 0.04 µmol.W^{-1}.h^{-1}), respectively.

Since these HER rates are normalized with respect to the surface area and the light flux (see SI, Section B-3.1), this enhancement is explained by the increase of the photo-active surface by a factor 2 and by the confinement of water in a small volume (4 mm-thick water layer, Figure 4c).[19]

Finally, a Solar-to-Hydrogen (STH) efficiency of 0.06% (see SI, Section B-4 and Section B-5) is obtained for the T-PC device from a salted water medium under a high pressure of 1.8 bar, which is very promising in comparison with the highest STH efficiency measured to date by Domen *et al.* for a particulate large-scale panel (STH 0.4%) involving more expensive and toxic materials (Sr, Cr).[19,38]

The robustness of the T-PC device with ethanol-water or salted water media was investigated over 5 days of illumination (Figure 4d, see SI, Section B-3.4). For either aqueous medium, two successive photocatalytic regimes are evidenced.

In the ethanol-water medium, water is first photo-reduced into H_2 whereas ethanol is oxidized into acetic acid, thus inducing a progressive decrease of the pH from 7.0 to 5.0 after 5 days of UV-visible illumination (equations 1-3). Acetic acid is indeed formed as byproduct of the reaction, as detected at the outcome of the photocatalytic experiment, likely through the intermediacy of acetaldehyde, albeit undetected (see SI, Section B-3.5). The pH variation, possibly accompanied by adsorption of acetic acid onto the catalyst surface induces a break in HER leading to a second regime in which no H_2 production takes place from 40 h to 5 days of illumination (Figure 4d, see SI, Figure S10). A too high content of acetic acid thus stops the H_2 production from water with the TiO_2/Au/TiO_2/Cbz PC material but does not affect the ability of the latter to produce H_2 again with a similar rate after refilling the T-PC device with a fresh ethanol-water solution at pH 7 (see SI, Figure S11).[45] This shows that the possible detrimental adsorption of acetic acid onto the catalyst surface is reversible (physisorption instead of chemisorption).

$$2\ H^+ + 2\ e^- \leftrightarrows\ H_2 \qquad (1)$$

$$CH_3CH_2OH + H_2O + 2\ p^+ \leftrightarrows\ CH_3COOH + H_2 + 2\ H^+ \qquad (2)$$

$$CH_3CH_2OH + H_2O \leftrightarrows\ CH_3COOH + 2\ H_2 \qquad (3)$$

With salted water, the behavior of the T-PC device is quite different. A first photocatalytic regime is observed until 80 h of irradiation (Figure 4d, see SI, Figure S10). Then, the normalized HER rate increases from 1.9 to 9.9 $\mu mol.W^{-1}.h^{-1}$ giving rise to the second photocatalytic regime while the pH increases progressively to 8.5 between 100 and 120 h (Figure 4d, see SI, Figure S10). The increase in pH is attributed to the formation of hypochlorite ions ClO^- (pK_a(HClO) = +

7.5) resulting from the oxidation of the chloride ions Cl^- (pK_a(HCl) < 0), thus acting as hole scavengers (equations 4-6):[46-48] in turn, the increase in pH induces an enhancement of the H_2 production rate (Figure 4d).[49]

$$2\ H^+ + 2\ e^- \leftrightarrows H_2 \qquad (4)$$

$$Cl^- + H_2O + 2\ p^+ \leftrightarrows ClO^- + 2\ H^+ \qquad (5)$$

$$Cl^- + H_2O \leftrightarrows ClO^- + H_2 \qquad (6)$$

Then, the stability of the T-PC device was investigated over 5 days of simulated day and night alternation in both ethanol-water and salted water media (Figure 4e-f). The photocatalytic H_2 production was thus monitored during 8 h of illumination, and 16 h of darkness, chosen to represent a day/night cycle. For both media, no significant loss of catalytic activity is observed in the H_2 production after 5 cycles, revealing the stability of the triptych bilayer photocatalyst under UV-visible illumination at room temperature and high pressure (1.8 bar). The coverage of the material surface by a photosensitive layer of Cbz ensures the stability of the photocatalyst (Figure 1). In the absence of Cbz layer, indeed the stability of the TiO_2 semiconductor film drastically decreases because of the photo-corrosion (see SI, Section B-6). In addition to its specific optoelectronic properties,[27,29] the Cbz photosensitizer, deposited as a thin layer, thus protects the TiO_2 surface from photo-corrosion.[26,50,51]

Finally, the triptych TiO_2/Au/TiO_2/Cbz material integrated in a device exhibits a high robustness (> 120 h) and stability (> 5 days) and thus, even under harsh conditions such as high pressure (1.8 bar) and salted water, which is over the state of art in the field (see SI, Table S1).

In summary, a simple combination of several components (TiO_2 + Au NPs + Cbz) enables exploiting a substantial part of the solar spectrum for efficient unassisted water photo-reduction. For the first time, deposition of a photocatalytic material on both the front glass and the back of a PC device allows increasing the photoactive surface area by a factor 2, thus enhancing the H_2 production rate in a significant manner. The performances of the novel T-PC device, working under relatively high pressure (1.8 bar), is particularly remarkable, when filed with salted water, giving a maximum Solar-To-Hydrogen efficiency (STH) of 0.06%. The use of seawater is not only essentially cheap and earth-abundant, but also key to the performance of the device: the NaCl content plays the role of a hole scavenger having a synergic effect on the hydrogen production rate (factor 5.2) through the pH increase resulting from its oxidation to NaOCl.

The T-PC device is shown to exhibit a remarkable stability due to a protecting effect of the thin photosensitive Cbz layer against photo-corrosion.[50,51] The high robustness of the device over at least 5 days under harsh conditions of high pressure (1.8 bar) and salted water, is indeed beyond the state of the art in the field of water splitting.

Finally, the disclosed design and manufacturing process is fully compatible with a large-scale development and adapted to commercial applications.

Experimental Section:

Sample preparation. The fabrication of the triptych bilayer material is described in Section A of the Supporting Information, and was adapted from procedures reported in the litterature.[26,29,52,53] A first layer of TiO_2 (270 nm and 1070 nm-thick) is sputter deposited by direct current magnetron sputtering on the silicon and glass substrates, respectively. The Au nanoparticles are synthesized from the gold salt precursor $HAuCl_{4.3}H_2O$ aqueous solution (50 mL, 2.5×10^{-4} mol/ L), the stabilizing agent sodium citrate in water (5 mL, 0.05 mol/ L) and the sacrificial agent (ethanol, 5 mL) under UV irradiation (l = 365 nm, 100 W, 30 min). The grafting of the Au nanoparticles onto the TiO_2 layer and the removal of the stabilizing agent are accomplished at the same time during the annealing under air at 200 °C during 10 min. A second layer of 270 nm-TiO_2 is then deposited by direct magnetron sputtering as previously described. Finally, a photosensitive layer of Cbz is deposited by immersion of the sample in an anisole solution of Cbz (2 mL, 0.5 mg/L) under stirring at 100 rpm on a shaker platform to give the triptych bilayer TiO2/Au/TiO2/Cbz hybrid nanomaterial depicted in Figure 1b.

Characterization. The characterization methods include scanning electronic microscopy (SEM), high-angle annular dark-field scanning transmission electronic microscopy (HAADF-STEM), energy dispersive X-ray spectrometry (EDS), grazing incidence X-ray diffraction (GI-XRD) X-ray photoelectron spectroscopy (XPS), ultraviolet-visible spectroscopy (UV-vis) and contact angle measurements, as detailed in Section A-2 of Supporting Information.

Photocatalysis. Each sample was immersed in 10 mL of the studied aqueous solution in a quartz reactor and irradiated by a solar simulator (Xenon lamp, 300 W) for 3 days. The reactor was connected to a gas chromatography (GC) system to measure (every 6 h) the hydrogen

production during the photo-reduction of water (see SI, Figure S1). A similar procedure is used for the T-PC device, as detailed in Section A-3 of Supporting Information.

Acknowledgement

All the synthesis and characterization were supported by the Region Occitanie (project MHytyque). This work was supported by LAAS-CNRS technology platform, a member of Renatech network. We thank the European Commission and Region Occitanie for their FEDER support (THERMIE grant) having partially funded the sputter-deposition equipment. We also thank the European Research Council as well as the Université Fédérale de Toulouse for its financial support through the PyroSafe project (grant number 832889). The authors thank Mehdi Djafari-Rouhani for his advices, Fabien Mesnilgrente, Véronique Conédéra, for their technological support, Xavier Dollat for the compartment fabrication of the H_2 PC device, Sarah Bailly for the synthesis of precursors of *carbo*-benzene molecules, Claudie Josse (Centre de Microcaractérisation Raimond Castaing) for the preparation of lamellas, the lifeguard Morgane Cocq for the sample of seawater.

Author Contributions

J. C. prepared the triptych materials, performed all the H_2 production measurements and directed and supervised the research. K. C. performed and supervised the synthesis of the photo-sensitive *carbo*-benzene molecule and provided support for the manuscript preparation; A. N. developed the deposition of the TiO_2 layers; K. T. performed the XPS characterization; T. H. realized the transmission electron microscopy observations of the lamellas; S. A.-S. realized the design and conception of the photocatalytic device; S. V. and L. S. optimized the PVD process for the TiO_2 deposition; M. Q.-L. provided support for the XPS characterization; V. M. and R. C.

provided support for the synthesis of carbo-benzene molecules and the manuscript preparation. A. E. provided support for the manuscript preparation. C. R. directed and supervised the research with J. C.

Competting financial interests

The authors declare no competing financial interests.

Corresponding author

Correspondance to: Jeremy Cure, jcure@laas.fr & Carole Rossi, carole.rossi@laas.fr

TOC Figure

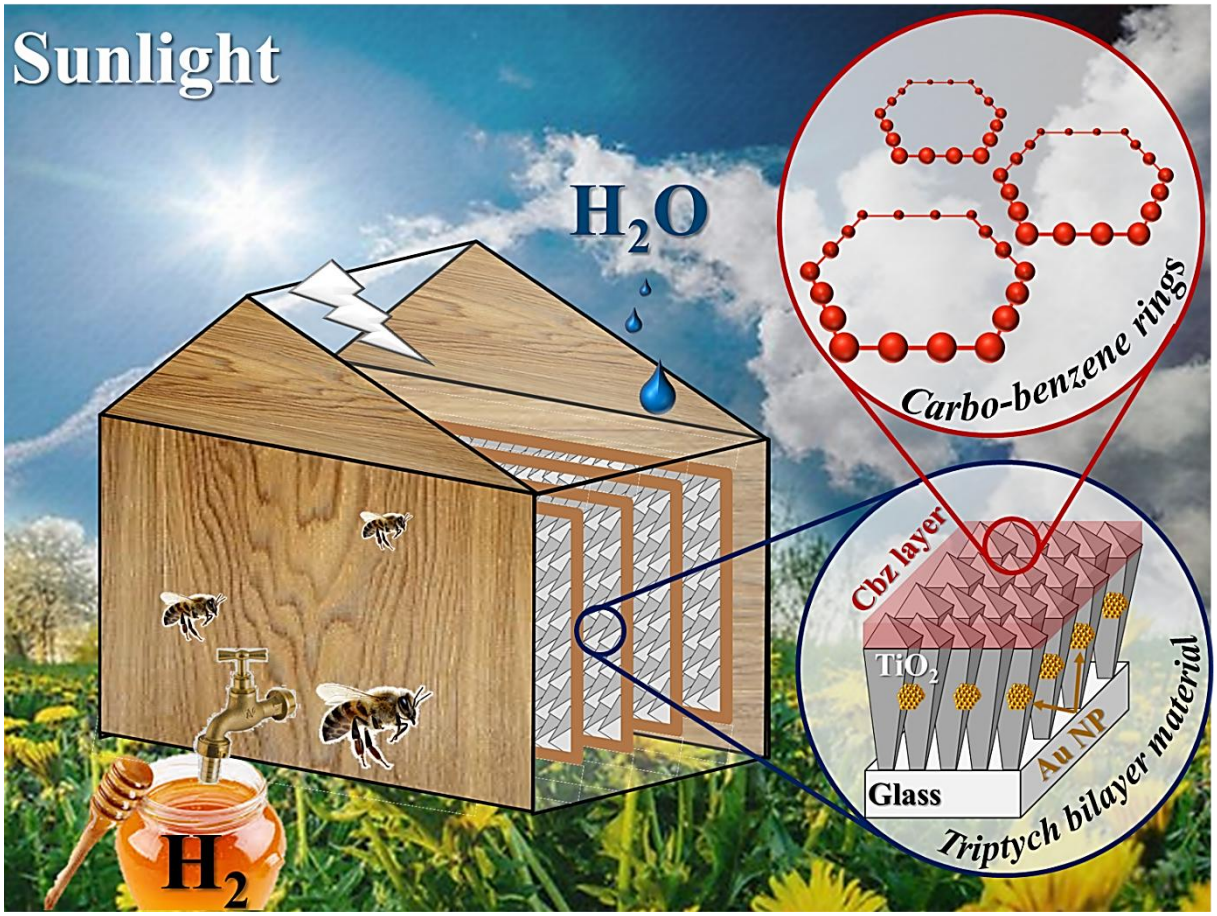
Sunlight
H_2O
H_2
Carbo-benzene rings
Cbz layer
TiO_2
Au NP
Glass
Triptych bilayer material

References

1 *10th Stakeholder Forum - Fuel Cell and Hydrogen Technology: Europe's Journey to a Greener World*. (2017).

2 Dutta, S. A review on production, storage of hydrogen and its utilization as an energy resource. *J. Ind. Eng. Chem.* **20**, 1148-1156 (2014).

3 ADEME. the Role of Hydrogen in the Energy Transition. *Technical review*, 1-15 (2018).

4 Pinaud, B. A. *et al.* Technical and economic feasibility of centralized facilities for solar hydrogen production via photocatalysis and photoelectrochemistry. *Energy Environ. Sci.* **6**, 1983-2002 (2013).

5 Balat, M. & Balat, M. Political, economic and environmental impacts of biomass-based hydrogen. *Int. J. Hydrogen Energ.* **34**, 3589-3603 (2009).

6 Acar, C. & Dincer, I. A review and evaluation of photoelectrode coating materials and methods for photoelectrochemical hydrogen production. *Int. J. Hydrogen Energ.* **41**, 7950-7959 (2016).

7 Dotan, H. *et al.* Decoupled hydrogen and oxygen evolution by a two-step electrochemical-chemical cycle for efficient overall water splitting. *Nature Energy* **4**, 786-795 (2019).

8 May, M. M., Lewerenz, H.-J., Lackner, D., Dimroth, F. & Hannappel, T. Efficient direct solar-to-hydrogen conversion by in situ interface transformation of a tandem structure. *Nat. Commun.* **6**, 8286 (2015).

9 Sivula, K. & Van de Krol, R. Semiconducting materials for photoelectrochemical energy conversion. *Nature Reviews Materials* **1**, 15010 (2016).

10 Abdi, F. F. *et al.* Efficient solar water splitting by enhanced charge separation in a bismuth vanadate-silicon tandem photoelectrode. *Nat. Commun.* **4**, 2195 (2013).

11 Luo, J. *et al.* Bipolar membrane-assisted solar water splitting in optimal pH. *Adv. Energy Mater.* **6**, 1600100 (2016).

12 Ager, J. W., Shaner, M., Walczak, K., Sharp, I. D. & Ardo, S. Experimental demonstrations of spontaneous, solar-driven photoelectrochemical water splitting. *Energy Environ. Sci.* **8**, 2811-2824 (2015).

13 Prevot, M. S., Guijarro, N. & Sivula, K. Enhancing the Performance of a Robust Sol-Gel-Processed p-Type Delafossite CuFeO2 Photocathode for Solar Water Reduction. *ChemSusChem* **8**, 1359-1367 (2015).

14 Fujishima, A. & Honda, K. Electrochemical Photolysis of Water at a Semiconductor Electrode. *Nature* **238**, 37-38 (1972).

15 Hisatomi, T., Kubota, J. & Domen, K. Recent advances in semiconductors for photocatalytic and photoelectrochemical water splitting. *Chem. Soc. Rev.* **43**, 7520-7535 (2014).

16 Wang, Z., Li, C. & Domen, K. Recent developments in heterogeneous photocatalysts for solar-driven overall water-splitting. *Chem. Soc. Rev.* **48**, 2109-2125 (2018).

17 Maeda, K. *et al.* Photocatalyst releasing hydrogen from water. *Nature* **440**, 295 (2006).

18 Marchal, C. *et al.* Au/TiO2-gC3N4 Nanocomposites for Enhanced Photocatalytic H2 Production from Water under Visible Light Irradiation with Very Low Quantities of Sacrificial Agents. *Adv. Energ. Mater.* **8**, 1702142 (2018).

19 Goto, Y. *et al.* A Particulate Photocatalyst Water-Splitting panel for Large-Scale Solar Hydrogen Generation. *Joule* **2**, 509-520 (2018).

20 Nalajala, N., Patra, K. K., Bharad, P. A. & Gopinath, C. S. Study on thin film form of a photocatalyst is better than the particulate form for direct solar-to hydrogen conversion. *RSC Adv.* **9**, 6094-6100 (2019).
21 Schröder, M. *et al.* Hydrogen Evolution Reaction in a Large-Scale Reactor using a Carbon Nitride Photocatalyst under Natural Sunlight Irradiation. *Energ. Technol.* **3**, 1014-1017 (2015).
22 Takata, T. & Domen, K. Particulate Photocatalysts for Water Splitting: Recent Advances and Future Prospects. *ACS Energ. Lett.* **4**, 542-549 (2019).
23 Melvin, A. A. *et al.* M-Au/TiO2 (M = Ag, Pd, and Pt) nanophotocatalyst for overall solar water splitting: role of interfaces. *Nanoscale* **7**, 13477-13488 (2015).
24 Tian, Y. & Tatsuma, T. Mechanisms and applications of plasmon-induced charge separation at TiO2 films loaded with gold nanoparticles. *J. Am. Chem. Soc.* **127**, 7636-7637 (2005).
25 Peng, Y. *et al.* Large-scale, low-cost, and high-efficiency water-splitting system for clean H2 generation. *ACS Appl. Mater. & Interfaces* **11**, 3971-3977 (2019).
26 Cure, J. *et al.* A triptych photocatalyst based on the co-integration of Ag nanoparticles and carbo-benzene dye into a TiO2 thin film. *Int. J. Hydrogen Energ.* **44**, 26347-26360 (2019).
27 Li, Z. *et al.* Towards graphyne molecular electronics. *Nat. Commun.* **6**, 6321 (2015).
28 Cocq, K., Lepetit, C., Maraval, V. & Chauvin, R. Carbo-aromaticity and novel carbo-aromatic compounds. *Chem. Soc. Rev.* **44**, 6535-6559 (2015).
29 Cocq, K., Barthes, C., Rives, A., Maraval, V. & Chauvin, R. Synthesis of Functional Carbo-benzenes with Functional Properties: The C 2 Tether Key. *Synlett* **30**, 30-43 (2019).
30 Esposito, D. V. *et al.* Photoelectrochemical reforming of glucose for hydrogen production using a WO3-based tandem cell device. *Energy Environ. Sci.* **5**, 9091-9099 (2012).
31 Hellstern, T. R. *et al.* Molybdenum Disulfide Catalytic Coatings via Atomic Layer Deposition for Solar Hydrogen Production from Copper Gallium Diselenide Photocathodes. *ACS Appl. Energy Mater.* **2**, 1060-1066 (2019).
32 Alrobei, H., Kumar, A. & Ram, M. K. Aluminum-a-hematite thin films for photoelectrochemical applications. *Surf. Rev. Lett.* **25**, 1950031 (2018).
33 Agarwal, D. *et al.* Engineering Localized Surface Plasmon Interactions in Gold by Silicon Nanowire for Enhanced Heating and Photocatalysis. *Nano Lett.* **17**, 1839-1845 (2017).
34 Wang, Q. *et al.* Particulate Photocatalyst Sheets Based on Carbon Conductor Layer for Efficient Z-Scheme Pure-Water Splitting at Ambient Pressure. *J. Am. Chem. Soc.* **139**, 1675-1683 (2017).
35 Okemoto, A. *et al.* Application of picene thin-film semiconductor as a photocatalyst for photocatalytic hydrogen formation from water. *Appl. Catal. B* **192**, 88-92 (2016).
36 Dal'Acqua, N. *et al.* Characterization and Application of Nanostructured Films Containing Au and TiO2 Nanoparticles Supported in Bacterial Cellulose. *J . Phys. Chem. C* **119**, 340-349 (2015).
37 Chauhan, M. *et al.* Promising visible-light driven hydrogen production from water on a highly efficient CuCo2S4 nanosheet photocatalyst. *J. Mater. Chem. A* **7**, 6985-6994 (2019).
38 Wang, Q. *et al.* Printable Photocatalyst Sheets Incorporating a Transparent Conductive Mediator for Z-Scheme Water Splitting. *Joule* **2**, 2667-2680 (2019).
39 Rojas, H. C. *et al.* All Solution-Processed, Hybrid Organic-Inorganic Photocathode for Hydrogen Evolution. *ACS Omega* **2**, 3424-3431 (2017).
40 Miquelot, A. *et al.* TiO2 nanotree films for the production of green H2 by solar water splitting: From microstructural and optical characteristics to the photocatalytic properties. *Appl. Surf. Sci.* **494**, 1127-1137 (2019).
41 Wang, T. M., Zheng, S. K., Hao, W. C. & Wang, C. Studies on photocatalytic activity and transmittance spectra of TiO2 thin films prepared by r.f. magnetron sputtering method. *Surf. Coat. Tech.* **155**, 141-145 (2002).

42 Denisov, N., Yoo, J. E. & Schmuki, P. Effect of different hole scavengers on the photoelectrochemical properties and photocatalytic hydrogen evolution performance of pristine and Pt-decorated TiO2 nanotubes. *Electrochim. acta* **319**, 61-71 (2019).
43 M., Y., Matsumoto, T. & Yamashita, T. Sacrificial hydrogen production over TiO2-based photocatalysts: Polyols, carboxylic acids, and saccharides. *Renew. Sust. Energ. Rev.* **81**, 1627-1635 (2018).
44 Zhang, J.-Y. *et al.* Energy-Saving Hydrogen Production Coupling Urea Oxidation over a Bifunctional Nickel-Molybdenum Nanotube Array. *Nano Energy* **60**, 894-902 (2019).
45 Imizcoz, M. & Puga, A. V. Optimising hydrogen production via solar acetic acid photoreforming on Cu/TiO2. *Catal. Sci. Technol.* **9**, 1098-1102 (2019).
46 Gao, M., Connor, P. K. N. & Ho, H. W. Plasmonic photothermic directed broadband sunlight harnessing for seawater catalysis and desalination. *Energy Environ. Sci.* **9**, 3151-3160 (2016).
47 Iguchi, S., Teramura, K., Hosokawa, S. & Tanaka, T. Effect of the chloride ion as a hole scavenger on the photocatalytic conversion of CO2 in an aqueous solution over Ni-Al layered double hydroxides. *Phys. Chem. Chem. Phys.* **17**, 17995-18003 (2015).
48 Kumaravel, V. & Abdel-Wahab, A. A Short Review on Hydrogen, Biofuel, and Electricity Production Using Seawater as a Medium. *Energy Fuels* **32**, 6423-6437 (2018).
49 Assi, H. *et al.* Triptych photocatalyst integrating TiO2 and Ag nanoparticles with a very thin layer of carbo-benzene dye for hydrogen photocatalytic production from water. *Manuscript in preparation* (2020).
50 Das, C. *et al.* Electron-selective TiO2 / CVD-Graphene Layers for Photocorrosion Inhibition in Cu2O Photocathodes. *Adv. Mater. Interfaces* **4**, n/a (2017).
51 Tang, Y., Hu, X. & Liu, C. Perfect Inhibition of CdS photocorrosion by graphene sheltering engineering on TiO2 nanotube array for highly stable photocatalytic activity. *Phys. Chem. Chem. Phys.* **16**, 25321-25329 (2014).
52 Cure, J. *et al.* Controlled Growth and Grafting of High-Density Au Nanoparticles on Zinc Oxide Thin Films by Photo-Deposition. *Langmuir* **34**, 1932-1940 (2018).
53 Leroyer, L., Zou, C., Maraval, V. & Chauvin, R. Synthesis and stereochemical resolution of a [6] pericyclynedione: Versatile access to pericyclynediol precursors of carbo-benzenes. *Comptes Rendus Chimie* **12**, 412-429 (2009).